VPS VIBRATIONS IN PHYSICAL SYSTEMS

DOI: 10.21008/j.0860-6897.2021.1.10
Vibrations in Physical Systems, 32(1):2021110, 2021

Influence of Cavity Edges Shape on Flow Induced Noise

Paweł ŁOJEK[1], Katarzyna SUDER-DĘBSKA[1], Michał MACH

Corresponding author: Paweł ŁOJEK, email: lojek@agh.edu.pl

[1] AGH University of Science and Technology, Department of Power Systems and Environmental Protection Facilities, 30 Mickiewicza Av., 30-059 Kraków, Poland

Abstract In this paper, impact of the cavity shape on flow-generated noise is analysed. As reference model, the classic rectangular cavity with perpendicular corners was used. The impact of both upstream and downstream edges was analyzed. In this paper, authors used hybrid method, where the flow was computed by means of Spalart-Allmaras Detached Eddy Simulations (DES) model, and the acoustic wave propagation was calculated by Curle acoustic analogy.

Keywords: aeroacoustics, computational fluid dynamics, cavity noise

1. Introduction

The problem of noise generation by the flow over cavity is important due to how often simple model of cavity can be used to analyze complex objects. With cavities, the flow phenomena occurring in landing gear, hatches of aircraft, valves and branches in ducts, elements of trains and cars, can be easily modelled [1]. Most research regarding cavities are limited to high flow velocities [2], while phenomena ocurring in incompressible range are not so well analyzed [3]. However, the noise generated with low velocity flow over cavities, for example in ventilation ducts, may be a significant problem. It is necessary to study the influence of various factors that affect the noise.

In this paper, the influence of the shape of the cavity on the generated noise is discussed. This is an issue already under research, however, as mentioned before, for velocities greater than those found in ventilation ducts [4,5]. Here we have analyzed the flow over 5 different geometric models of the cavity and acoustic pressure generated by it.

The flow over cavity is described by incompressible time-dependent Navier-Stokes equations, solved with finite volume method and PIMPLE algorithm used by OpenFoam solver. The analyzed velocities allow the assumption that the flow was turbulent Spalart Allmaras DES model was used to solve the turbulent flow. The acoustic pressure was computed by Lighthill's acoustic analogy.

1. Methodology

1.1. Flow modelling

The equations used to describe the flow were the continuity (1) and Navier-Stokes equation (2) [6]:

$$\frac{\partial \rho}{\partial t} + \frac{\partial}{\partial x_i}(\rho v_i) = 0, \tag{1}$$

$$\frac{\partial}{\partial t}(\rho v_i) + \frac{\partial}{\partial x_j}(\rho v_j v_i) = f_i, \tag{2}$$

where ρ – density, v_i – velocity in i direction, f_i – external forces in i direction.

Assuming simplifications such as fluid incompressibility and Stokes hypothesis [7], the equations (1, 2) takes the form:

$$\frac{\partial v_i}{\partial x_i} = 0, \tag{3}$$

$$\frac{\partial v_i}{\partial t} + v_j \frac{\partial v_i}{\partial x_j} = -\frac{1}{\rho}\frac{\partial p}{\partial x_i} + \nu \nabla^2 v_i, \tag{4}$$

where: p – pressure, $\nu = \mu/\rho$ – kinematic viscosity coefficient.

1.2. Turbulence modelling

In cases where the flow is turbulent, it is practically impossible to solve the above equations numerically in a direct manner using direct numerical simulations (DNS). In this study, we used hybrid method, called Detached Eddy Simulation (DES). This method combines Reynolds-Averaged Navier-Stokes (RANS) and Large Eddy Simulation (LES) methods, depending on the size of the computational mesh. Methods mentioned above are described in greater detail in [7].

The RANS method is based on the decomposition of the flow into a time-averaged part and random fluctuations The incompressible continuity (3) and Navier-Stokes (4) equations takes the form [7]:

$$\frac{\partial \overline{v}_i}{\partial x_i} = 0, \tag{5}$$

$$\rho \frac{\partial \overline{v}_i}{\partial t} + \rho \overline{v}_j \frac{\partial \overline{v}_i}{\partial x_j} = -\frac{\partial \overline{p}}{\partial x_i} + \frac{\partial}{\partial x_j}\left(\overline{\tau}_{ij} + \tau_{ij}^R\right), \tag{6}$$

where $\phi = \overline{\phi} + \phi'$, $\overline{\phi}$ – time-averaged variable, ϕ' – fluctuating variable, $\overline{\tau}_{ij} = \mu\left(\frac{\partial \overline{v}_i}{\partial xj} + \frac{\partial \overline{v}_j}{\partial x_i}\right)$ – viscous stress tensor, $\tau_{ij}^R = -\rho\overline{v'_i v'_j}$ – Reynolds stress tensor.

Reynolds stress tensor τ_{ij}^R introduces new unknown variables, that must be modelled to solve the equations. The most common solution to this problem (called the closure problem) is to use the Boussinesq hypothesis. It allows to determine the Reynolds tensor according to [7]:

$$\tau_{ij}^R = 2\mu_T\left(\frac{\partial \overline{v}_i}{\partial x_j} + \frac{\partial \overline{v}_j}{\partial x_i}\right) - \frac{2}{3}\rho k \delta_{ij}, \tag{7}$$

where: k – turbulence kinetic energy, μ_T – turbulent viscosity.

The turbulent viscosity is determined on the basis of additional equations resulting from the assumed turbulence model, in this case – Spalart-Allmaras model [8]. This model is based on transport equation for a viscosity-like variable $\hat{\nu}$.

The model equation is given by:

$$\frac{\partial \hat{\nu}}{\partial t} + v_j \frac{\partial \hat{\nu}}{\partial x_j} = c_{b1}(1 - f_{t2})\hat{S}\hat{\nu} - \left[c_{w1} f_w - \frac{c_{b1}}{\kappa^2} f_{t2}\right]\left(\frac{\hat{\nu}}{d}\right)^2 = \frac{1}{\sigma}\left[\frac{\partial}{\partial x_j}\left((\nu + \hat{\nu})\frac{\partial \hat{\nu}}{\partial x_j}\right) + c_{b2}\frac{\partial \hat{\nu}}{\partial x_i}\frac{\partial \hat{\nu}}{\partial x_i}\right], \tag{8}$$

where: $\hat{\nu}$ – model variable – eddy viscosity, $c_{b1}, c_{w1}, c_{b2}, \kappa, \sigma,$ – constants of the model, $f_w, f_{t2}, \hat{S}$ – additional functions, described in [8].

Turbulent viscosity μ_T required by Boussinesq assumption given by eq. (7) is calculated according to the formulas (9), (10), (11):

$$\mu_T = \rho \hat{\nu} f_{v1}, \tag{9}$$

$$f_{v1} = \frac{\chi^3}{\chi^3 - 7.1}, \tag{10}$$

$$\chi = \frac{\hat{\nu}}{\nu}. \tag{11}$$

The LES method is based on spatial filtering, the flow variables are decomposed on part solved numerically (eddies larger than $\hat{\Delta}$) and modelled part. After decomposition the continuity (3) and Navier-Stokes (4) equations takes the form [9]:

$$\frac{\partial \overline{v}_i}{\partial x_i} = 0, \tag{12}$$

$$\frac{\partial \overline{v}_i}{\partial t} + \frac{\partial}{\partial x_j}\left(\overline{v}_i \overline{v}_j\right) = -\frac{1}{\rho}\frac{\partial \overline{p}}{\partial x_i} + \nu \nabla^2 \overline{v}_i - \frac{\partial \tau_{ij}^S}{\partial x_j}, \tag{13}$$

where: $\phi = \overline{\phi} + \phi'$, $\overline{\phi}$ – filtered variable, ϕ' – modelled variable, $\tau_{ij}^S = \overline{v_i v_j} - \overline{v}_i \overline{v}_j$ – subgrid scale stress (SGS) tensor.

The SGS tensor describes the effect of scales smaller than $\hat{\Delta}$ and must be modeled to be able to solve the closure problem and the equations themselves.

In the case of the DES hybrid method, the model used to compute the SGS tensor is the Spalart-Allmaras turbulence model given by the equation (8). There is one significant change in the model itself, the distance from the nearest wall d is replaced by the value given by the equation [10]:

$$\tilde{d} = \min(d, C_{DES}\Delta), \tag{14}$$

where: $C_{DES} = 0.65$ – empirical constant, $\Delta = \max x, y, z$ – longest cell edge.

1.3. Acoustic analogies

The noise generated by the flow was calculated from the acoustic analogies that were formulated by Lighthill [11], given by [12]:

$$\frac{\partial^2 \rho'}{\partial t^2} - c_\infty^2 \frac{\partial^2 \rho'}{\partial x_i^2} = \frac{\partial^2 T_{ij}}{\partial x_i \partial x_j}, \tag{15}$$

where: p' – acoustic pressure, c_∞ – speed of sound, $T_{ij} = \rho v_i v_j + p_{ij} - c_\infty^2 \rho \delta_{ij}$ – Lighthill tensor.

This equation assumes that sound is created as a result of flow in an unbounded space. The Lighthill equation alone cannot therefore be used for noise calculations in the duct flow.

This equation was solved by Curle using the Green's method [13]. Curle assumed that although the acoustic wave does not interact with the walls, it can be generated by acoustic sources that arise due to the interaction of the flow with the walls [14]. The Curle equation is given by:

$$\rho'(\mathbf{x}, t) c_\infty^2 = \int_S \left[\frac{\partial \rho v_j}{\partial \tau}\right]_{\tau=\tau^*} \frac{n_j \mathrm{d}S(\mathbf{y})}{4\pi|\mathbf{x}-\mathbf{y}|} - \frac{\partial}{\partial x_i}\int_S \left[p_{ij} + \rho v_i v_j\right]_{\tau=\tau^*} \frac{n_j \mathrm{d}S(\mathbf{y})}{4\pi|\mathbf{x}-\mathbf{y}|} + \frac{\partial^2}{\partial x_i \partial x_j}\int_V \left[T_{ij}(\mathbf{y}, \tau)\right]_{\tau=\tau^*} \frac{\mathrm{d}V(\mathbf{y})}{4\pi|\mathbf{x}-\mathbf{y}|}. \tag{16}$$

Additionally, assuming simplifications, such as impermeable walls, an acoustically compact source and small Mach numbers, the equation takes the form [14]:

$$\rho'(\mathbf{x}, t) c_\infty^2 \approx \frac{x_i}{4\pi|\mathbf{x}|^2 c_\infty}\left[\frac{\partial F_i}{\partial \tau}\right]_{\tau=\tau*} \quad F_i(\tau) = \int_S p_{ij}\, n_j \mathrm{d}S(\mathbf{y}). \tag{17}$$

The equation in this form relates the time derivative of the forces acting on the walls due to flow with the acoustic pressure generated by the flow. It has been implemented and is available in the OpenFOAM software used to model the flows over the cavities.

2. Numerical modelling

2.1. Geometric model

The simulation of the flow over the cavities was carried out for five models, one of which was the reference model. It was a classical rectangular cavity with perpendicular corners (Fig. 1a), while the other models differed in shapes of the leading and trailing edges. Two cases with chamfered edges (Fig. 1b, 1c) and two with rounded edges (Fig. 1d, 1e). In each case, the cavities had the same geometric dimensions and a L/D ratio of 2. These dimensions are presented in Tab. 1.

Tab. 1. Dimensions of the model

L	D	h	l_1	l_2
0.4	0.2	0.6	0.15	1.5

The length of the computational domain behind the cavity resulted from the necessity to observe the turbulence and fluctuations that may occur as a result of the phenomena occurring in the cavity. The cavity itself was considered to be placed in a channel of height h and width equal to 0.3m. Due to the fact that the simulations were two-dimensional, the width of the channel was used only for the purpose of calculating the forces acting on the walls of the cavity and channel.

The rounding radius for the rounded cavities was 0.25D - 0.05m, while the chamfered corner cavities were cut at an angle of 45°, 0.05m from the corner.

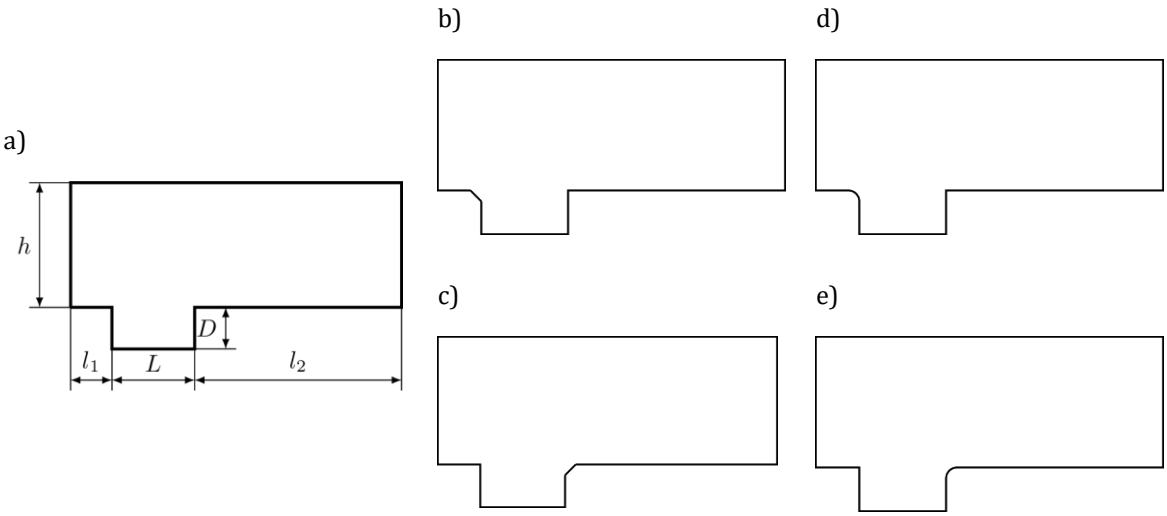

Fig. 1. Analyzed models of the cavity: a) reference model (RM), b) chamfered upstream edge (CUE), c) chamfered downstream edge (CDE) d) rounded upstream edge (RUE), e) rounded downstream edge (RDE).

2.2. Initial and boundary conditions

The modeled fluid was air at the temperature of 20°C, the density and kinematic viscosity of which were $\rho = 1.2$ kg/m and $\nu = 1.5 \cdot 10^{-5}$ m²/s.

It was necessary to define the initial conditions in the entire computational domain and the boundary conditions at individual boundaries. More precisely, the initial and boundary values of velocity v, pressure p, turbulent viscosity ν_T and parameter $\hat{\nu}$, resulting from the adopted Spalart-Allmaras turbulence model, had to be determined.

The domain could be divided into 4 types of boundaries: inlet, outlet, walls and the "empty" boundary. The empty condition was assumed on the front and back of the three-dimensional domain with one cell in thickness so that the model was treated as two-dimensional.

The initial and boundary condition values are presented in Tab. 2.

Tab 2. Initial and boundary conditions.

	Velocity v	Pressure p	Turbulent viscosity υ_T	Parameter $\hat{\nu}$
Inlet	$v_x = 10, v_{y,z} = 0$	$\frac{\partial p}{\partial x_n} = 0$	Calculated	$\hat{\nu} = 10^{-5}$
Outlet	$\frac{\partial v_{x,y,z}}{\partial x_n} = 0$	$p = 0$	calculated	$\hat{\nu} = 10^{-5}$
Walls	$v_{x,y,z} = 0$	$\frac{\partial p}{\partial x_n} = 0$	$\nu_T = 0$	$\frac{\hat{\nu}}{\partial x_n} = 0$
Internal domain	Initialized with potential flow solver	$p = 0$	$\nu_T = 0$	$\hat{\nu} = 10^{-5}$

3. Results and discussion

Acoustic pressure has been calculated using the equation (17) implemented directly in OpenFOAM. It was evaluated for the listener placed 5 m directly above the cavity (for center of coordinate system at upstream edge, the listener was placed at (0.2,5,0.15)). The sound pressure level L_p obtained after filtering the computed signal with finite impulse response filter and further processing is shown in Fig. 2. The obtained sound pressure levels for each case were also shown in third-octave bands in Tab. 3.

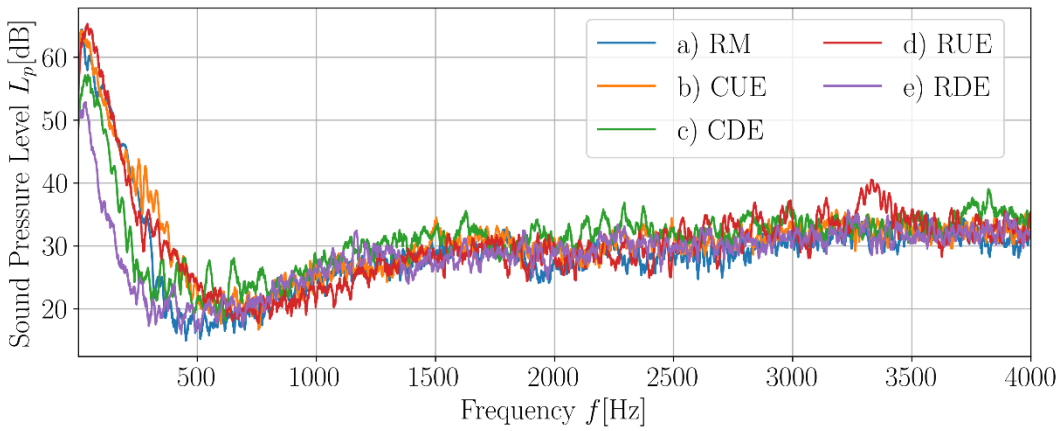

Fig. 2. Spectrum of sound pressure level for listener 5 m above the cavity, for different shapes.

The results confirm the preliminary assumption that the edge change may have a significant impact on the generated noise. As shown in Fig 2., changing the shape of the downstream edge of cavity helps to reduce noise, in comparison to reference edge. This is especially the case when a rounded downstream edge is used. In case of chamfered downstream edge, on the one hand, lower sound pressure levels are obtained, and on the other hand, especially in range of 400 ÷ 750 Hz, the SPL is greater compared to the reference model. The nature of the resulting fluctuations is also different, there is tonal noise in this range.

In the case of modified upstream edges, this change increases the sound pressure level compared to the reference model, both for rounded and chamfered edges.

Tab. 3. Third-octave band sound pressure level for listener 5 m above the cavity.

Central Frequency f_c [Hz]	Sound Pressure Level L_p [dB]				
	a) RM	b) CUE	c) CDE	d) RUE	e) RDE
16.00	74.27	74.44	63.24	71.33	62.12
31.50	74.69	76.61	69.02	77.42	65.01
63.00	74.55	76.29	70.54	79.18	62.86
125.00	72.09	71.14	66.10	73.86	54.48
250.00	62.87	63.66	51.97	60.70	45.79
500.00	44.60	51.42	49.08	50.40	45.50
1000.00	54.25	54.15	56.14	52.69	55.05
2000.00	60.73	62.29	63.19	61.23	60.91
4000.00	67.69	68.66	69.62	68.11	67.59
8000.00	74.17	75.03	75.93	74.45	74.03
16000.00	79.97	80.75	81.58	79.96	79.65

In Fig.3. the flow pressure and velocity distributions are shown. The different flow characteristics between particular edge shapes are clear, the size and distribution of vortices in the cavities differs, as well as the size and frequency of the detached vortices in downstream part of the duct.

In the case of chamfered downstream, rounded upstream and downstream edges, (models c), d), e)), two main vortices inside the cavity can be distinguished, the larger of which, at the downstream side of the cavity, covers about 70% of it's volume. For different time steps (not shown here) the behaviour of the vortices in the cavity looks similar – two main vortices can be distinguished, but their percentage share changes, up to 50% for each vortex. The only cavity that does not behave this way is cavity with chamfered upstream edge.

a) Pressure field – reference model

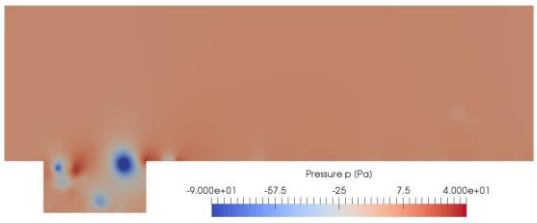

b) Velocity field – reference model

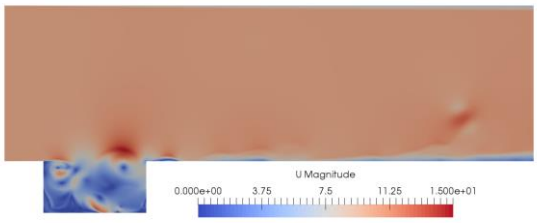

c) Pressure field. – chamfered upstream edge

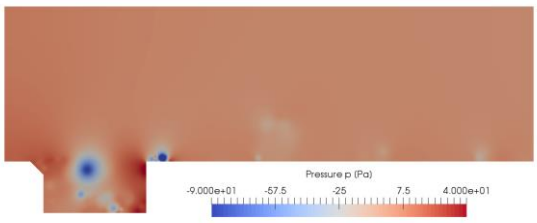

d) Velocity field – chamfered upstream edge

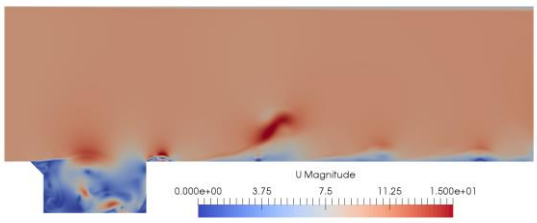

e) Pressure field – chamfered downstream edge f) Velocity field – chamfered downstream edge

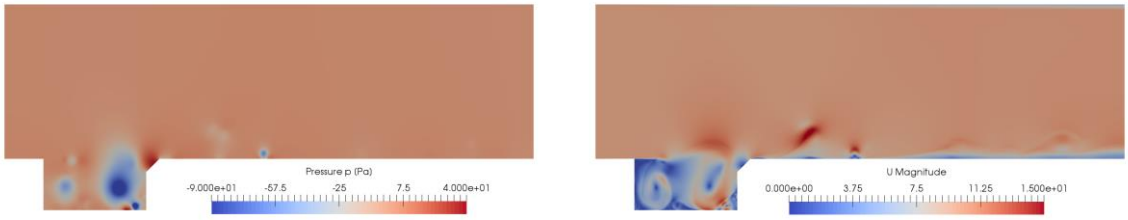

g) Pressure field – rounded upstream edge h) Velocity field – rounded upstream edge

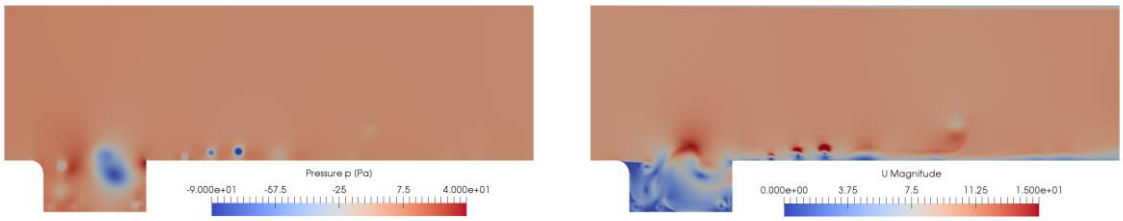

i) Pressure field – rounded downstream edge j) Velocity field– rounded downstream edge

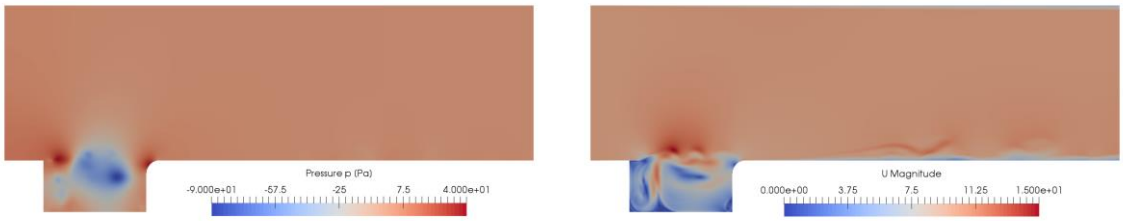

Fig. 3. Pressure and velocity distributions of the flow over cavities at time t = 1.2 s.

4. Conclusions

This work investigated the impact of cavity edges shape on flow-generated noise. Main goal of the study was to determine how acoustic pressure at the listener changes depending on the shape used. The flow-induced noise was computed using hybrid DES-Curle method.

The obtained results show that the change in the shape of the edges of the cavity has an impact on the formation of sound. This is especially true when changing the downstream edge. Change of downstream edge from perpendicular to rounded allowed to reduce the sound pressure level by approx. 10 dB. Change of the upstream edge, to both rounded and chamfered had no beneficial effect on the generated noise.

The results are encouraging for further work, both on analysing different edge and walls shapes and for applications. The future work will focus on the study of the various diameters of the fillet on the generated noise. Also, it should be tested, what will be the effect of changing both edges, in different configurations.

Acknowledgments

This research was supported in part by PLGrid infrastructure.

Additional information

The authors declare no competing financial interests.

References

1. D. Rockwell, E., Naudascher, Review – Self-Sustaining Oscillations of Flow Past Cavities, J. Fluids Eng. 100(2), 1978.
2. M.B. Tracy, E.B., Plentovich, Cavity Unsteady-Pressure Measurements at Subsonic and Transonic Speeds, Nasa Technical Paper 3669, 1997.
3. P. Lafon, S. Caillaud, J.P. Devos, C., Lambert. Aeroacoustical coupling in a ducted shallow cavity and fluid/structure effects on a steam line, Journal of Fluids and Structures, 18(6), 2003.
4. G.B. Ashcroft, K. Takeda, X. Zhang. A numerical investigation of the noise radiated by a turbulent flow over a cavity, Journal of Sound and Vibration, 265(1):43-60, 2003,
5. H. Kim, Z. Hu, D. Thompson. Numerical investigation of the effect of cavity flow on high speed train pantograph aerodynamic noise, Journal of Wind Engineering & Industrial Aerodynamics, 201:104159 2020.
6. F. Moukalled, L. Mangani, M. Darwish. The Finite Volume Methods in Computational Fluid Dynamics. An Advanced Introduction with OpenFOAM and Matlab, Springer Science+Business Media, 2016.
7. J. Blazek, Computational Fluid Dynamics. Principles and Applications, Elsevier Ltd., 2015.
8. P. R. Spalart, S. R. Allmaras. A One-Equation Turbulence Model for Aerodynamic Flows, Recherche Aerospatiale, 1:5-21, 1994.
9. P. Sagaut. Large Eddy Simulation for Incompressible Flows. An Introduction. Springer Science+Business Media, 2006.
10. P. R. Spalart, W. H. Jou, M. Strelets, S. R. Allmaras. Comments on the feasibility of LES for wings and on a hybrid RANS/LES approach, 1st AFOSR Int. Conf. on DNS/LES, Aug. 4-8, 1997.
11. M. J. Lighthill, M. H. Newman. On sound generated aerodynamically I. General theory, Proceedings of the Royal Society of London. Series A. Mathematical and Physical Sciences, 211(1107), 1952.
12. S. Glegg, W. Devenport. Aeroacoustics of Low Mach Number Flows. Fundamentals, Analysis and Measurement, Elsevier Inc., 2017.
13. N. Curle. The Influence of Solid Boundaries upon Aerodynamic Sound, Proceedings of the Royal Society A, 231, 505-514, 1955.
14. I. Czajka. Modelowanie zjawisk akustycznych w przepływach aerodynamicznych, Wydawnictwa AGH, 2019.